METALS AND MATERIALS International, Vol. 8, No. 3 (2002), pp. 271~281

Analysis of Mixed Grade Transition in Continuous Thin Slab Casting with EMBR

J. H. Ahn, J. K. Yoon and Jung-Eui Lee*

School of Materials Science and Engineering, Seoul National University
San 56-1 Sillim-dong, Gwanak-gu, Seoul 151-742, Korea
*Steelmaking Research Group, Technical Research Lab., POSCO
1 Goe-dong, Nam-gu, Pohang 790-785, Korea

A concentration change during grade transition operation in thin slab casting is investigated through computer simulation and the results are compared with experimental measurements. Fluid flow and mixing patterns in various tundish levels and flow rates were analyzed by a three-dimensional mathematical model. Based on the contained results, a simple, efficient and accurate computational model is suggested to predict the concentration profile at the outlet of the tundish. Based on the model, mixing in and below the mold was analyzed considering electromagnetic braking force. The predicted concentration profiles show good agreements with the measured values. It is found that the lower vortices in the mold are suppressed by the electromagnetic field and a plug-like flow region develops, which decreases the intermixing of two different grades of steel and shortens the length of transition region.

Keywords : grade transition, thin slab casting, tundish, mold, EMBR

1. INTRODUCTION

Continuous casting become world-widely adopted in the steel industry due to its tremendous advantages over the traditional ingot casting process in terms of energy savings, higher yield and flexibility of operation. Efforts have been made continuously to improve the quality of the cast products, reduce costs and thus increase the competitiveness of the steel manufacturer. One way to reduce costs is to minimize the amounts of intermixed steel during the grade transition operation.

There are several different procedures in handling the casting of dissimilar grades for the continuous casting. Each method produces different amounts of intermixed steel and incurs different costs. The flying tundish method changes the tundish before the ladle with new grade steel is opened. Thus, intermixed steel is produced only by the mixing of two grades in the strand. In addition, a grade-separator can be inserted into the mold to further decrease such mixing. The ladle change method continuously casts the dissimilar grades as a single sequence. This completely reduces any losses in productivity, produces maximum amounts of intermixed slab among the grade transition methods. In order to choose the best method for a particular operation, many researches have been conducted [1-4]. Fig. 2 shows the schematic diagram of thin slab caster of POSCO at Kwangyang considered in this study. Liquid core reduction is accomplished through segment 0 and the slab is thinned from 84.4 mm to 67.5 mm. Through the reduction units (RU1, RU2), the slab is further reduced to a bar shape with a thickness of 20-30 mm. The bar is cut by shear pendulum with the length of at least 50 m. The significant features of thin slab caster are high casting speed (3.6 m/min-4.4 m/min) and thinness of mold compared to conventional slab caster. In the case of present continuous thin slab caster of POSCO mini mill, the only possible method is to change ladle during the grade transition due to the plant operation conditions of high casting speed and small mold thickness. For the case of slab caster, it is general to slow down casting speed during ladle exchange. By doing so, it promotes more solidification in the strand which, in turn, shortens liquid pool where two grades will mix. But for the case of thin slab caster, it is reported that many defects appear if the variation of casting speed exceeds 0.3 m/min.

During ladles exchange, the tundish with the old grade of steel being cast is first emptied in a certain level of depth while the flow rate out of the tundish keeps constant according to the casting speed and slab dimensions. Once the new ladle opens, the new grade steel is usually poured at a rate greater than the steady-state casting flow rate to refill the tundish to its normal operating level. During this process, the new grade steel flowing from the new ladle will mix with old

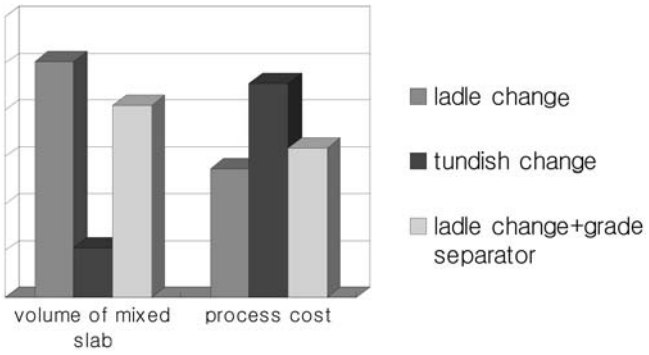

Fig. 1. Comparison of grade transition methods.

grade steel left in the tundish. Steel then flows into the mold, where it undergoes further mixing in the long liquid pool in the strand while it solidifies.

There being no device to decrease intermixing between two grades, lots of mixing occurs during ladle exchange and, therefore, intermixed slabs are produced. Thus, the prediction of mixing during grade transition as a function of casting conditions is very important in minimizing downgrading and to avoid unintentional delivery of mixed grade products to customers.

In this research, the grade transition by ladle change method for EMBR installed thin slab casting process was studied. Through a three-dimensional coupled analysis of fluid flow

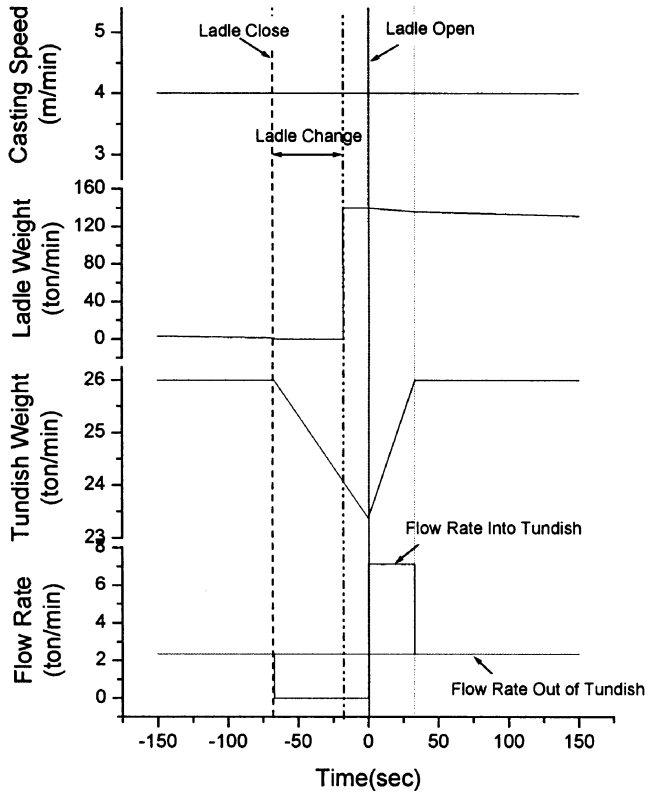

Fig. 3. Change of ladle weight, tundish weight and flow rates with time during a grade transition (POSCO).

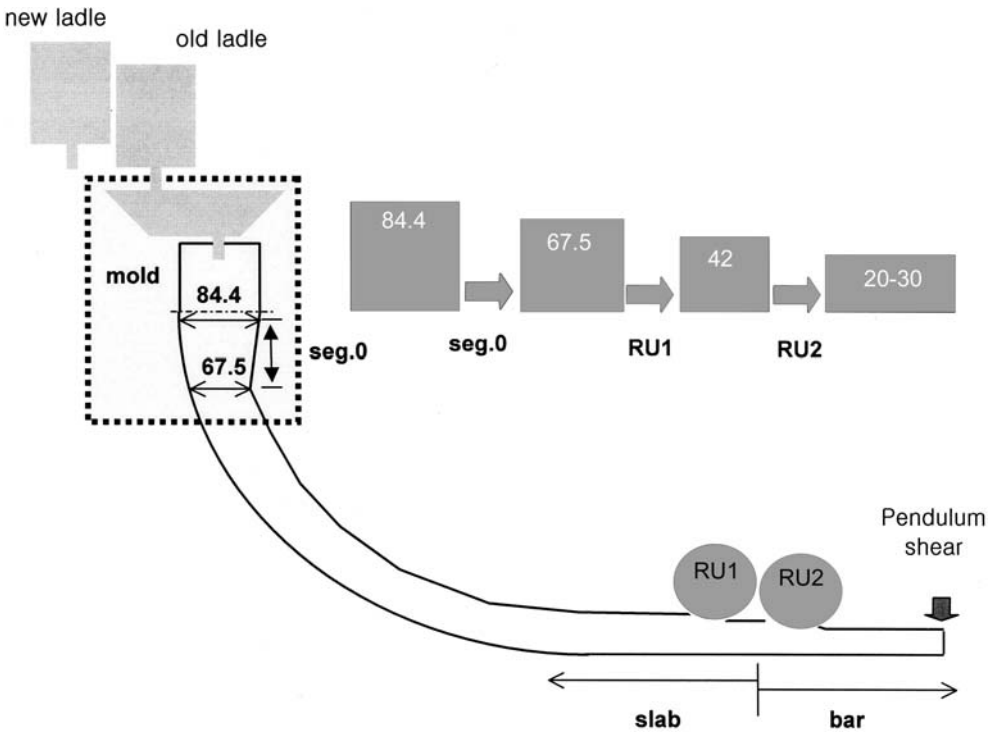

Fig. 2. Diagram of the continuous thin slab casting process.

and heat transfer, the mixing of dissimilar grades was investigated as a function of casting parameters such as casting speed and tundish working level. Using these results, simple computational model was developed to determine the concentration history of steel entering into the mold. After the mixing in the strand was analyzed, the amounts of intermixed slabs were predicted. It should be noted that in this work, transient effect on the fluid flow in the tundish and thermal effect on the fluid flow in the strand were ignored. These effects will be considered in the following publications.

2. MATHEMATICAL MODEL

The system selected for the present investigation is a thin slab caster tundish and mold. Fig. 4 shows a half longitudinal section of the tundish with two weirs (T-shape and Π-shape) as the flow modification devices. The normal operating depth of the tundish is 1.0 m. This corresponds to a full tundish capacity of approximately 26 metric tons. A schematic diagram of the mold is shown in Fig. 5.

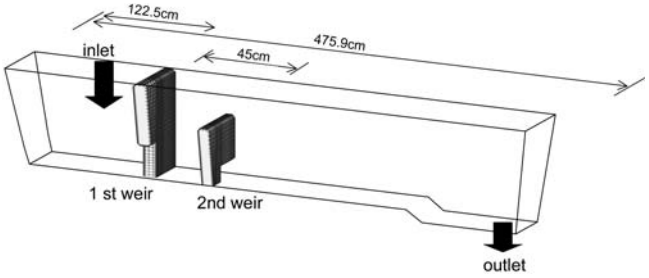

Fig. 4. Schematic representation of a half of tundish.

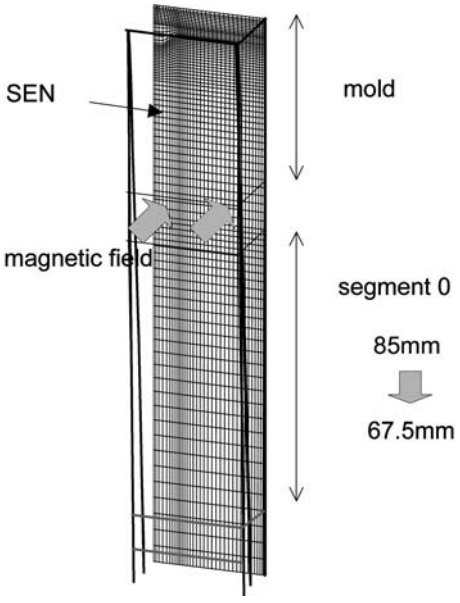

Fig. 5. Schematic representation of one quarter of mold and strand.

Major assumptions in this study are as follows.

1. The casting speed and tundish working level were kept constant during grade transition process
2. Strand was not curved.
3. The thickness of solidified cell was proportional to the square root of distance from the meniscus and solidified cell moved with casting speed.
4. Elements mixed equally.

From the above mentioned assumptions, the inlet and outlet velocity were fixed along the casting speed and slab dimensions and the flow fields in the tundish and mold were at a steady state.

To include the effect of solidified shell on molten steel flow, the grid system was constructed consistently with the liquid core region using solidification constant K obtained from the experimental data. After calculating steady state flow field coupled with induced current density, mixing in the strand was analyzed.

2.1. Formulation

The governing equations of mass, momentum, energy and species for an incompressible fluid are written in tensor form.

$$\frac{\partial(\rho u_i)}{\partial x_i} = 0 \tag{1}$$

$$\frac{\partial(\rho u_i u_j)}{\partial x_j} = -\frac{\partial p}{\partial x_i} + \frac{\partial}{\partial x_j}\left[\mu_{eff}\left(\frac{\partial u_i}{\partial x_j} + \frac{\partial u_j}{\partial x_i}\right)\right] + \rho_{ref} g_i \beta(T - T_{ref}) + F_{m,i} \tag{2}$$

$$\frac{\partial(\rho c u_i T)}{\partial x_i} = \frac{\partial}{\partial x_i}\left(k_{eff}\frac{\partial T}{\partial x_i}\right) \tag{3}$$

$$\frac{\partial(\rho C)}{\partial t} + \frac{\partial(\rho u_i C)}{\partial x_i} = \frac{\partial}{\partial x_i}\left(D_{eff}\frac{\partial C}{\partial x_i}\right) \tag{4}$$

The last term in Eq. 2 is the i-th component of electromagnetic braking force,

$$\vec{F}_m = \vec{J} \times \vec{B} \tag{5}$$

where $\vec{J}$ and $\vec{B}$ are electric current density and magnetic flux density, respectively.

Viscosity that appears in Eq. 2 means the enhanced quantity by turbulent eddy motion described as

$$\mu_{eff} = \mu_m + \mu_t \tag{6}$$

where μ_m and μ_t are molecular and turbulent viscosity of fluid, respectively.

The turbulent viscosity is calculated from k-ε turbulent model as

$$\mu_t = \rho C_\mu \frac{k^2}{\varepsilon} \tag{7}$$

k_{eff} in Eq. 3 is the effective thermal conductivity of molten steel calculated as

$$k_{eff} = k_m + k_t \tag{8}$$

where k_m and k_t are molecular and turbulent thermal conductivity.

D_{eff} in Eq. 4 is effective diffusivity calculated as

$$D_{eff} = D_m + D_t \tag{9}$$

where D_m and D_t are molecular and turbulent diffusivity.

Once the turbulent viscosity is known, the turbulent thermal conductivity and diffusivity may be deduced from

$$k_t = \frac{\mu_t}{\sigma_t} \tag{10}$$

$$D_t = \frac{\mu_t}{\sigma_c} \tag{11}$$

where σ_t and σ_c are the turbulent Prandtl and Schmidt numbers, respectively.

The governing equations of turbulent kinetic energy, k, and its dissipation rate, ε, are given by :

$$\frac{\partial}{\partial x_i}\left(\rho u_i k - \frac{\mu_{eff}}{\sigma_k}\frac{\partial k}{\partial x_i}\right) = G - \rho\varepsilon \tag{12}$$

$$\frac{\partial}{\partial x_i}\left(\rho u_i \varepsilon - \frac{\mu_{eff}}{\sigma_\varepsilon}\frac{\partial \varepsilon}{\partial x_i}\right) = (C_1\varepsilon G - C_2\rho\varepsilon^2)/k \tag{13}$$

where

$$G = \mu_t \frac{\partial u_i}{\partial x_i}\left(\frac{\partial u_i}{\partial x_j} + \frac{\partial u_j}{\partial x_i}\right) \tag{14}$$

In this study C is defined as

$$C \equiv \frac{F(t) - F_{old}}{F_{new} - F_{old}} \times 100 \tag{15}$$

where F(t) is the fraction of a given element in the alloy and F_{old} and F_{new} are the fractions of that element measured in the old and new grades, respectively. In this definition, all concentrations range between the old grade concentration of 0 and new grade concentration of 100.

The electric current density induced in the moving conducting fluid under magnetic field is given by the following Ohm's equation as

$$\vec{J} = \sigma(\vec{E} + \vec{V} \times \vec{B}) \tag{16}$$

where σ is the electrical conductivity.

In foregoing equation, electric field intensity $\vec{E}$ can be expressed as gradient of scalar variable by introducing electrical potential ϕ.

$$\vec{J} = \sigma(-\nabla\phi + \vec{V} \times \vec{B}) \tag{17}$$

In Eq. 17, $\vec{B}$ is given as the initial data and $\vec{V}$ is calculated from momentum equation at the previous iteration step. The induced current should satisfy the continuity equation.

$$\nabla \cdot \vec{J} = 0 \tag{18}$$

Substitution of Eq. 17 into Eq. 18 gives

$$\nabla^2\phi = \nabla \cdot (\vec{V} \times \vec{B}) \tag{19}$$

2.2. Boundary conditions

The boundary conditions over the symmetric planes are the standard conditions of zero gradient for velocity, pressure and relative concentration, etc. At the outflow boundaries, zero gradient of normal velocity and relative concentration conditions are imposed. At the free surface, which was assumed to be flat, the normal of velocity, shear stress and normal mass flux are set to be zero. To ensure that the overall continuity is satisfied, the total mass flux going out of the computational domain is corrected to be equal to the total mass flux coming into the domain. The logarithmic law of wall was used to compute shear stresses. At the walls, no slip and zero species mass flux boundary conditions were imposed. For the modeling of the thermal conditions of liquid steel in the tundish, the incoming steel jet was considered to be at a constant temperature of 1843 K. At the walls and free surface, the fixed heat flux boundary conditions were used, which were taken from Chakraborty and Sahai [5]. For calculating induced electric field, meniscus and mold walls

Table 1. Heat losses from the tundish [5]

Free surfaces	15.00 kW/m^2
Longitudinal vertical wall	3.2 kW/m^2
Transverse vertical wall	3.8 kW/m^2
Bottom wall	1.4 kW/m^2
Walls of Flow control devices	1.75 kW/m^2

Table 2. Parameters for modeling of fluid flow and heat transfer

Slab width	1240 [mm]
Slab thickness	67.6 [mm]
Casting speed	3.6-4.4 [m/min]
Inlet area (tundish)	0.5×28.274 [cm^2]
Outlet area (tundish)	0.5(206.112 [cm^2]
Density	7020-0.702(T-T_{ref}) [kg/m^3]
Viscosity	0.0067 [kg/m · sec]
Specific heat capacity	710 [J/kg · K]
Thermal conductivity	33 [kg ·m/sec^3]

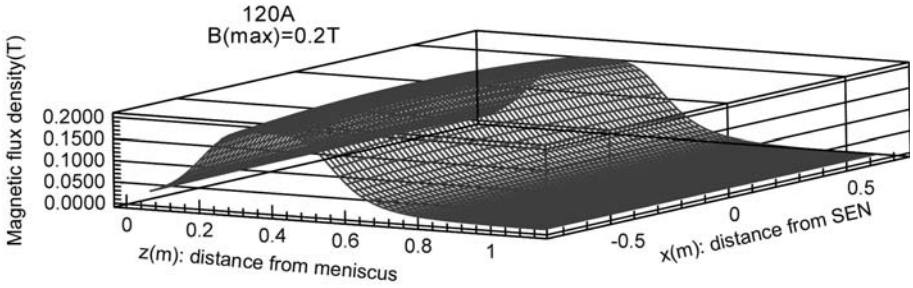

Fig. 6. Distribution of magnetic field used for calculating electromagnetic force.

were assumped to be electrically insulated. At symmetric planes and boundary at the end of strand, electrical potential, ϕ was set to be zero. Fig. 6 shows the distribution of magnetic flux density in the mold when impressed electric current is 120A. This magnetic field was used to calculate the electromagnetic braking force in the mold.

2.3. Numerical method

Finite difference equations were derived for the coupled governing partial differential equations using body fitted coordinates and solved by SIMPLE (Semi-Implicit Pressure Linked Equations) algorithm. To investigate the effects of height of steel in the tundish, calculations on 4 levels (70%, 80%, 90%, 100%) were carried out. Fig. 7 shows the flow domains corresponding to the symmetrical half of the tundish containing 4 different amounts of molten steel divided into a non-uniform grid of 128 (longitudinal)×24 (transverse)×32 (vertical). The inlet and outlet openings were roughly approximated as rectangular planes. Fig. 8 shows the symmetrical quarter of the mold and strand divided into a non-uniform grid of 60 (longitudinal)×18 (transverse)×86 (vertical). The length of the strand of 3.5 m was determined by trial and

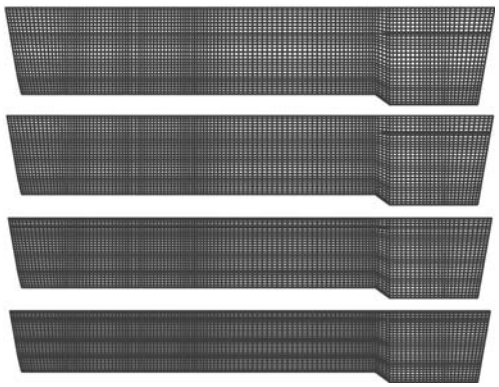

Fig. 7. Grid systems of the tundish with various heights of molten steel.

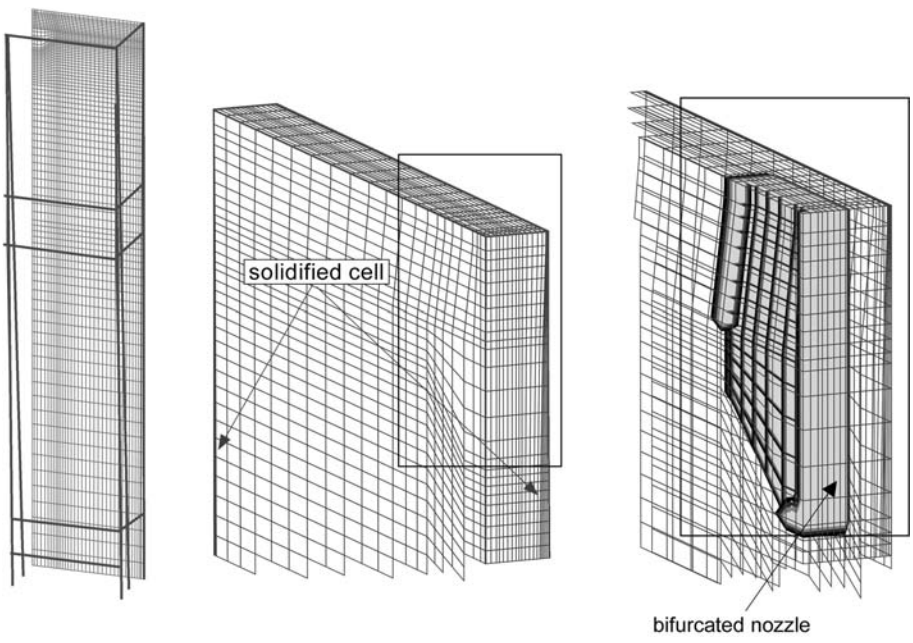

Fig. 8. Grid system of the mold and strand.

error. It was found that one directional fluid flow developed below this distance. After steady state flow fields were obtained, time dependent mixing patterns were calculated.

3. RESULTS AND DISCUSSION

Due to the high casting speed and small entry and holes of weirs compared to the size of tundish, heavy fluid mixing with high turbulence occurs before the 2nd weir (Π-shape). Fig. 9 presents an isometric view of the flows generated in a half section of the tundish operated at normal working level (100% WL) and 70% normal working level (70% WL). As seen, the entering jet hits the bottom of the tundish and then flows downstream through the hole of 1st weir (T-shape) or sideways towards and along the walls of the tundish. The liquid steel flowing underneath the weir moves vertically upwards towards the free surface between the two weirs. This flow then moves downstream towards the exit nozzle.

As shown in Fig. 10, the effect of casting speed on primary flows are negligible except that flows through the 2nd weir (Π-shape) hole occurs as casting speed increases. Fig. 11 shows the change of the velocity profiles with tundish working levels. As the WL decreases, the effect of incoming jet becomes more important and the velocities in the later part are increased. Fig. 12 shows the steady state temperature profiles corresponding to the velocity profiles shown in Fig. 11. It is interesting to note that the average temperature of tundish, presented as brightness, is lowest at 90% WL. This

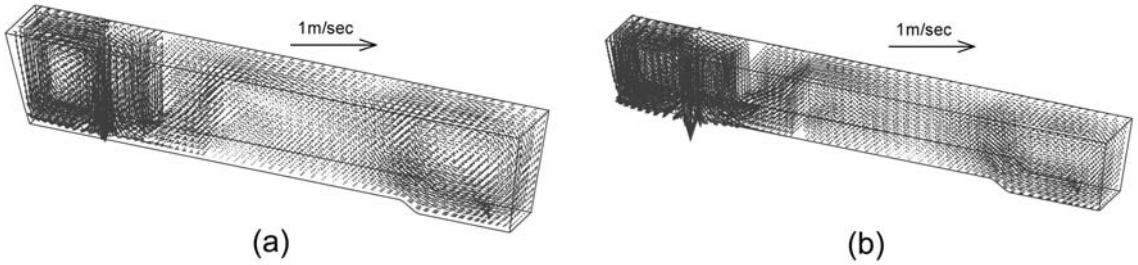

Fig. 9. An isometric view of flow fields predicted in the tundish (v_c= 4.0 m/min): (a) 100% WL; 70% WL.

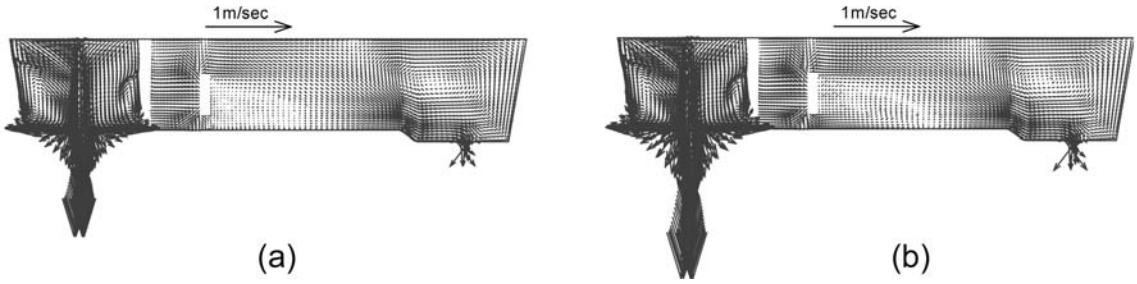

Fig. 10. Predicted flow field and its speed contour in symmetric longitudinal plane (v_c=4.0 m/min): (a) v_c=3.6 m/min; (b) v_c=4.4 m/min.

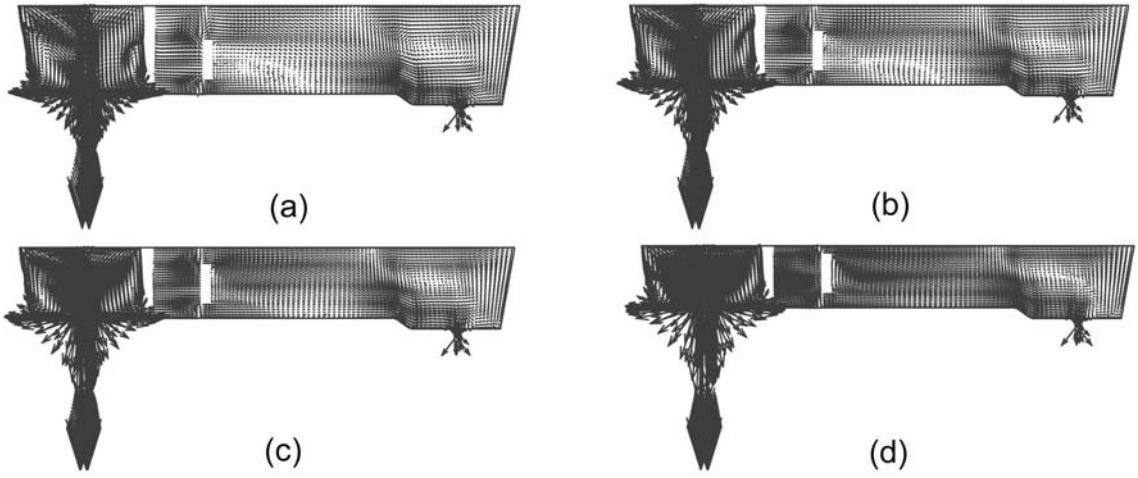

Fig. 11. Predicted flow field in symmetric longitudinal plane (v_c=4.0 m/min): (a) WL=100%; (b) WL=90%; (c) WL=80%; and (d) WL=70%.

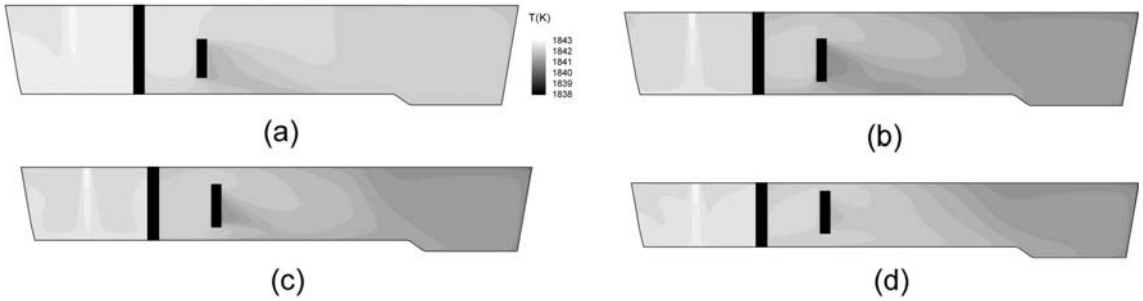

Fig. 12. Predicted temperature field in symmetric longitudinal plane (v_c=4.2 m/min): (a) WL=100%; (b) WL=90%; (c) WL=80%; and (d) WL=70%.

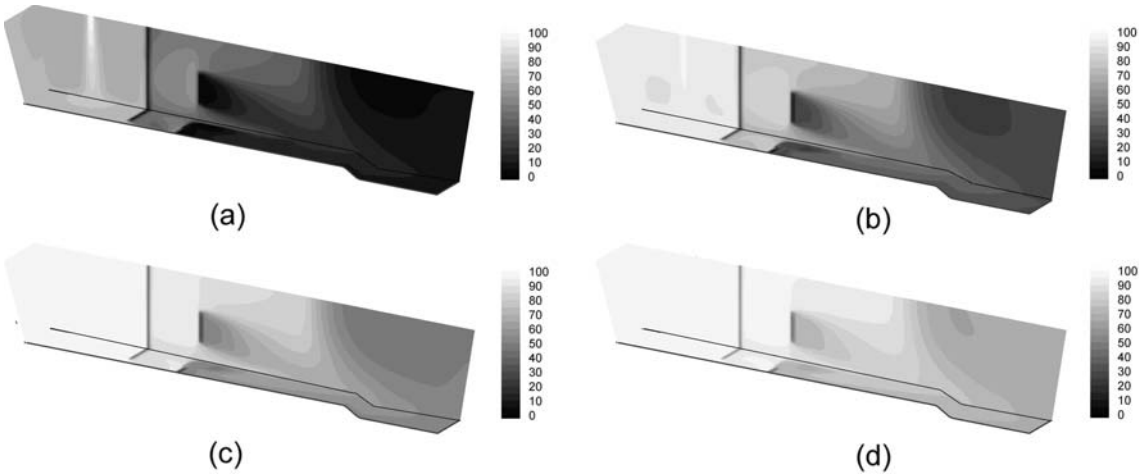

Fig. 13. Predicted relative concentration field in tundish (v_c=4.2 m/min, 100% WL): (a) time=200 sec; (b) time=400 sec; (c) time=600 sec; and (d) time=800 sec.

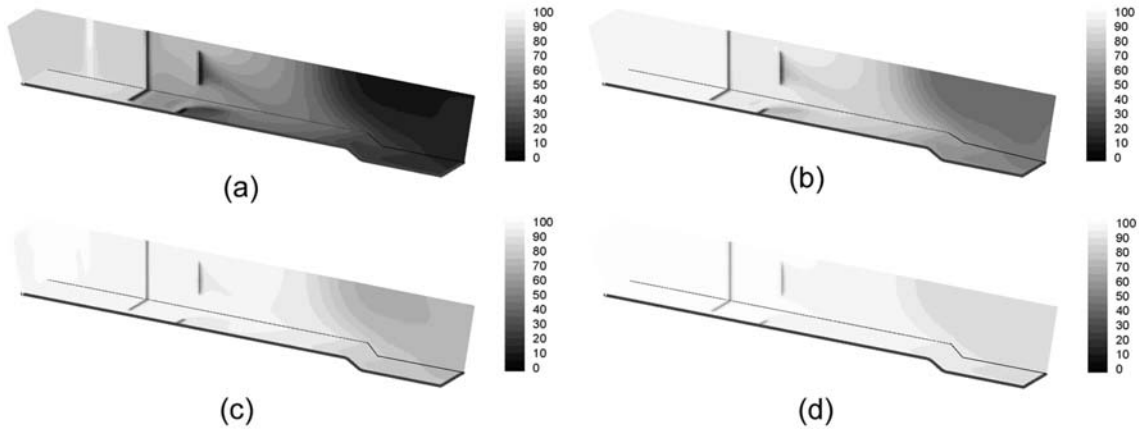

Fig. 14. Predicted relative concentration field in tundish (v_c=4.0 m/min, 70% WL): (a) time=200 sec; (b) time=400 sec; (c) time=600 sec; and (d) time=800 sec.

can be explained by the average heat loss introduced as the product of MRT (Mean Residence Time) and heat loss through the free surface and walls per unit time and unit volume. As WL decreases, MRT (interpreted as average time to be cooled) decreases, while heat loss per unit time and unit volume increases. So the average heat loss in the tundish has a maximum value where the average temperature has a minimum value as WL varies.

Based on calculated flow fields, mixing patterns were analyzed using a dimensionless or relative concentration defined in Eq. 15. Figs. 13 and 14 show time transient spatial distribution of 2nd molten steel with different composition poured

Table 3. Theoretical mean residence time (sec)

v_c(m/min)	3.6	3.8	4.0	4.2	4.4
70% WL	493	467	443	422	403
80% WL	572	541	514	489	468
90% WL	653	619	588	560	535
100% WL	738	699	634	632	604

at time zero. At 100% WL, most of the 2nd molten steel moves upward over the 2nd weir and dead zone develops near the backside wall of 2nd weir and wide face of tundish. On the other hand, lots of 2nd molten steel also flows through the hole of 2nd weir at 70% WL.

Fig. 15(a) shows the outlet concentration as a function of time for different tundish operation conditions. It is interesting to note that two different F-type RTD curves give almost identical normalized F-type RTD behavior as seen in Fig. 15(b). Although the local flow field and mixing pattern are different from one another, the overall mixing pattern in the tundish - perfect mixing before 2nd weir, plug flow-like behavior after 2nd weir - does not change. All predicted normalized RTD are shown in Fig. 16.

From the above results, a new grade composition entering into the mold can be modeled as a function of MRT. In this study, Boltzmann type curve fitting method is adopted to predict the composition history.

$$C = \frac{A_1 - A_2}{1 + e^{(\theta_{T/D} - \theta_0)/A_3}} + A_2 \tag{20}$$

where, $\theta_{T/D} = \frac{t}{MRT} = \frac{t}{V_{T/D}/Q_{T/D}}$, $Q_{T/D} = W \times T \times v_c$

A_1, A_2, A_3 are fitting parameters.

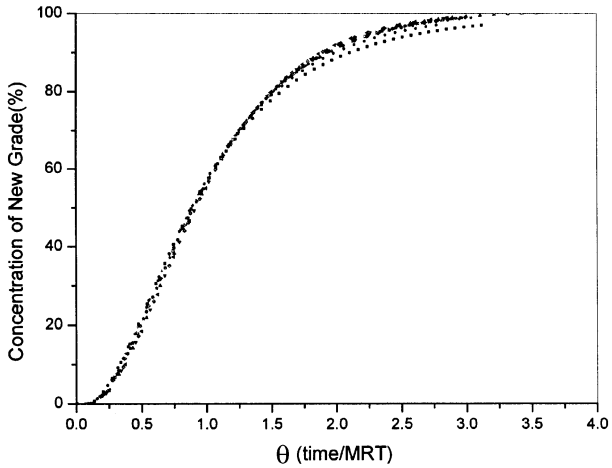

Fig. 16. Normalized RTD profiles.

To validate developed model of this study, concentrations of Mn are compared between experimentally measured value of sampled molten steel near the SEN (Submerged Entry Nozzle) and model prediction. The working level of tundish was kept 5% higher than the normal working level before the ladle change so as to compensate for the drop in the molten steel surface during the exchange of ladles. The relatively large difference in the initial stage is attributed to the abrupt pouring of molten steel which is not considered in this model.

The developed finite difference model has also been applied to account for the mixing in the mold. To consider the effect of magnetic field, Lorentz force is included in a Source term for momentum. Fig. 18(a) shows steady state fluid flow. Fig. 18(c) shows velocity contour at the end of calculation domain. It is remarkable 1-directional fluid flow region develops near the end of segment 0. Fig. 19 shows the

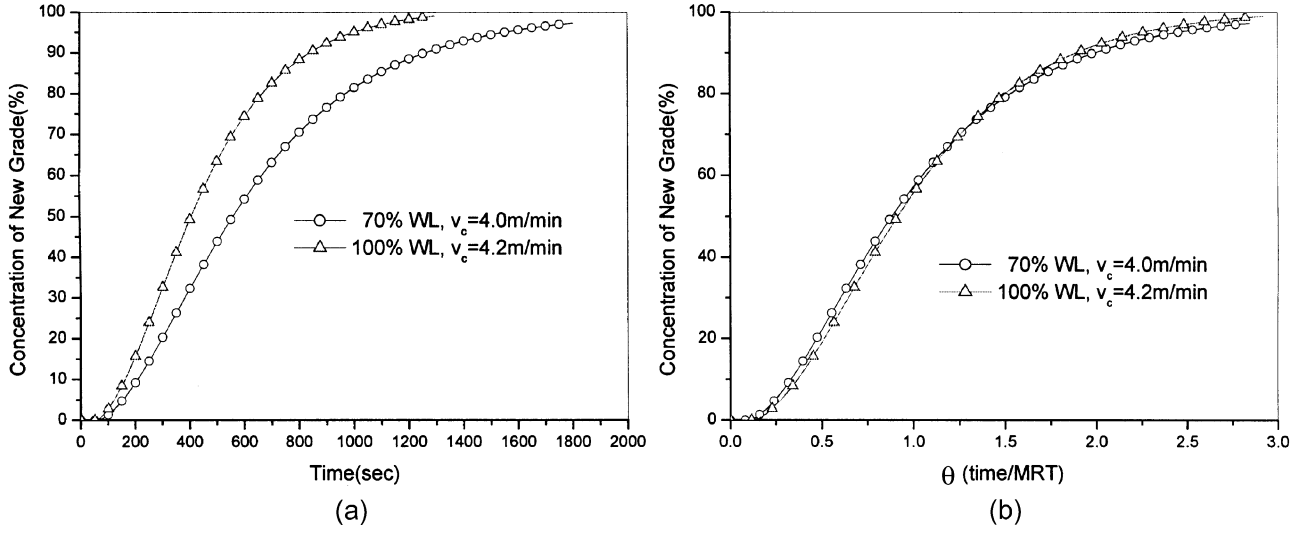

Fig. 15. Predicted RTD and normalized RTD profiles: (a) F-type RTD; (b) Normalized F-type RTD.

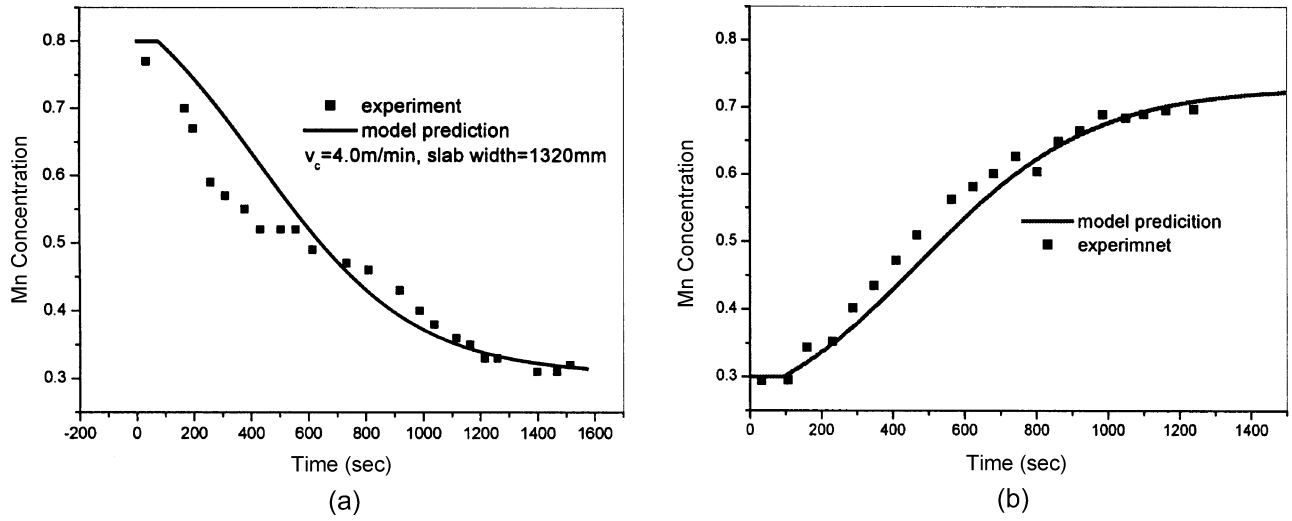

Fig. 17. Comparison of predicted Mn composition with measurements: (a) Experiment 1: Mn (0.8→0.3); (b) Experiment 2: Mn (0.3→0.73).

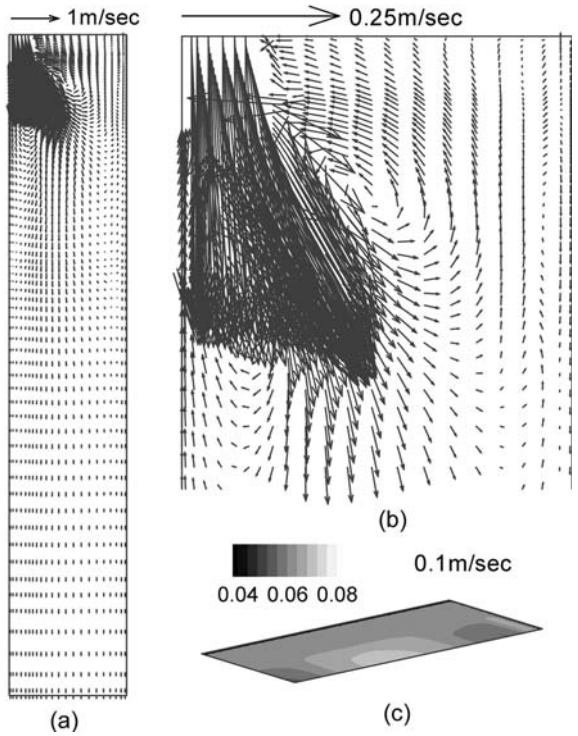

Fig. 18. Fluid flow in mold and strand (v_c=3.8 m/min).

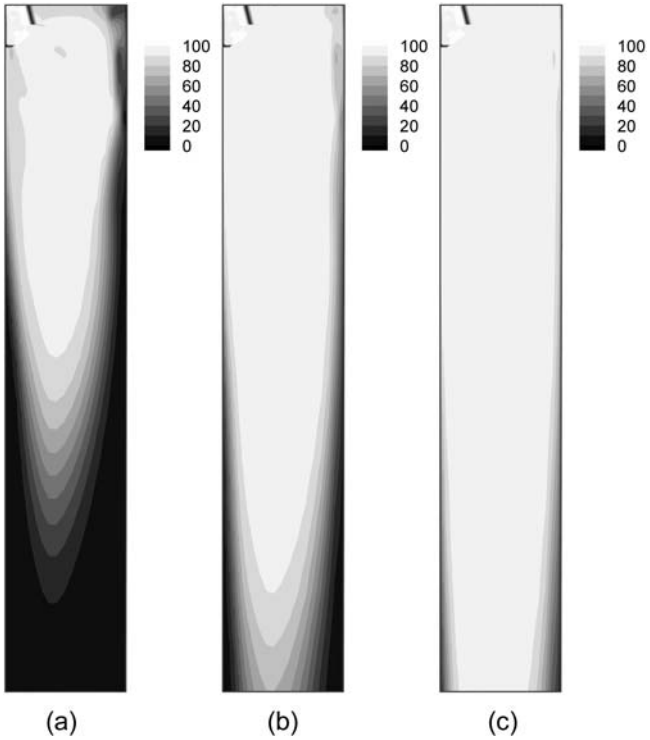

Fig. 19. Mixing Pattren in mold and strand (vv_c=3.8 m/min): (a) t=20 sec; (b) t=40 sec; and (d) t=40 sec.

mixing patterns when the inlet value of relative concentration remains at 100 from time of zero. This shows characteristics of the mixing in strand. As shown in Fig. 20, almost perfect mixing occurs in the mold due to high turbulence and recirculation. The model of composition in final product is the same as reference 4. In this model, mixing is assumed to proceed at each point in the strand until such time when that point solidifies. Fig. 20 shows predicted concentration history at the metallurgical length (10.6 m from the meniscus). The shapes of the composition history curves are the same. And at the equal distance from the meniscus, the history curves behave almost identically. The time difference among inlet history and the others merely corresponds to the time to travel 10.6 m at constant casting speed. This phenomenon can be explained by the flow field and the small volume of strand compared with tundish. As seen in Fig. 19, there are

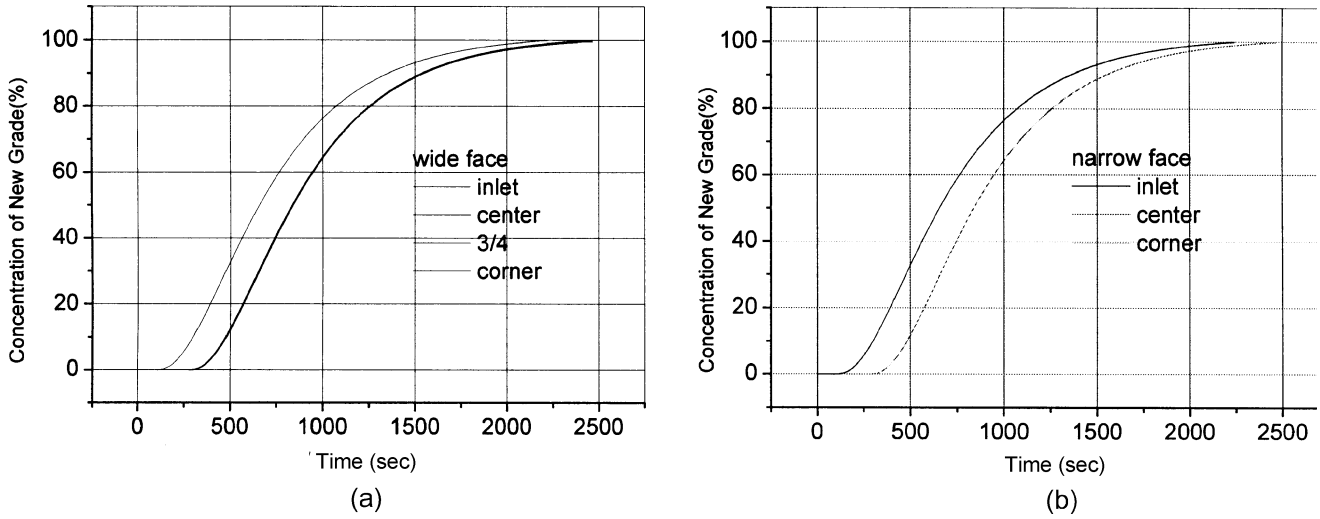

Fig. 20. Concentration history at the metallurgical length: (a) wide face and (b) narrow face.

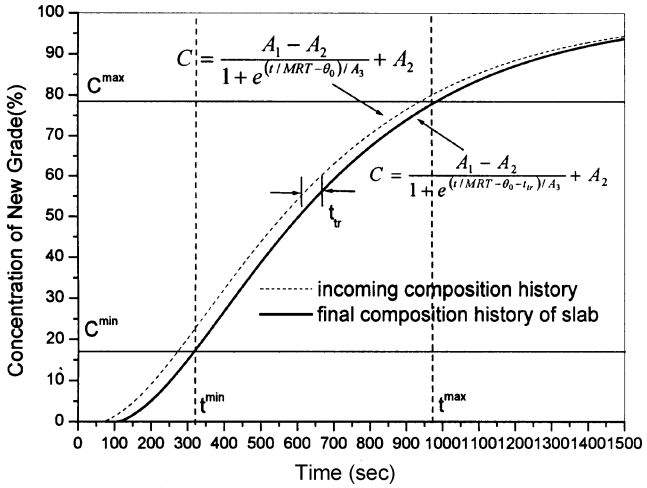

Fig. 21. Prediction of total inter-mixed slab.

heavy mixing region in the mold and plug-flow-like region near the end of segment 0. As the mold plays a role of a perfect mixing reactor due to the heavy mixing as well as small volume, the every history curves at a position in the mold are almost identical. And one directional fluid flow without recirculation below the mold keeps the shape of composition history curve.

From the above mentioned results, by introducing only one term to Eq. 20, the total amounts of mixed grade slab can be predicted. The final composition in the slab can be described as,

$$C = \frac{A_1 - A_2}{1 + e^{(t/MRT - \theta_0 - t_r)/A_3}} + A_2 \tag{21}$$

where t_r is the time to travel from the meniscus to the arbitrary point at the casting speed. The variables in Eq. 21 are MRT and t_r.

For example, the concentration of bar at shear pendulum can be predicted as follows.

$$t_r = \frac{d_1}{v_c} + \frac{d_2}{v_c \times \frac{67.5}{th_1}} + \frac{d_3}{v_c \times \frac{67.5}{th_2}} \tag{22}$$

d_1: distance between meniscus and RU1
d_2: distance between RU1 and RU2
d_3: distance between RU2 and shear pendulum
th_1: thickness of bar passing RU1
th_2: thickness of bar passing RU2

If the composition range of inter-mixed slab ($C^{min}<C<C^{max}$) is specified as relative concentration, the period when the concentration lies within that range can be obtained.

$$t^{min} = MRT \times \left[t_r + \theta_c + A_3 ln\left(\frac{A_1 - C^{min}}{C^{min} - A_2} \right) \right] \tag{23}$$

$$t^{max} = MRT \times \left[t_r + \theta_c + A_3 ln\left(\frac{A_1 - C^{max}}{C^{max} - A_2} \right) \right] \tag{24}$$

Then, the total volume of inter-mixed slab can be predicted as

$$Vol^{mix} = (t^{max} - t^{min}) \times v_c \times W \times T \tag{25}$$

Actually the amount predicted from Eq. 25 is the minimum amount due to the restriction of cutting process.

4. CONCLUSIONS

(1) Through a three-dimensional numerical analysis, a simple computational model was developed. This model can

predict final slab composition profiles corresponding to arbitrary casting conditions.

(2) Although the molten steel behavior and mixing patterns depend on the casting conditions, the composition history entering into the mold could be described as a function of MRT.

(3) When electromagnetic force is applied at the mold, the total volume of mixed grade steel depends only on the mixing in the tundish.

ACKNOWLEDGEMENT

This work was supported by the Technical Research Labs., POSCO. The authors would like to thank S. Y. Kim, Kwangyang Steel making Research Team, POSCO for their helpful discussions and sharing of data.

NOMENCLATURE

$\vec{B}$: magnetic flux density vector
$\vec{E}$: electric field intensity vector
$\vec{J}$: electric current density vector
$\vec{F}_m$: magnetic force
$\vec{V}$: velocity vector
u_i : velocity components
x_i : coordinates on physical domain
p : pressure
μ_l : laminar or molecular viscosity
μ_t : turbulent viscosity
μ_{eff} : effective viscosity
v_c : casting speed
W : width of thin slab
T : thickness of thin slab

REFERENCES

1. C. Damle and Y. Sahai, *Iron & Steelmaker* **22**, 6,49 (1995).
2. H. Chen and R. D. Pehlke, *Steelmaking Conf. Proc*., p. 695 (1994).
3. M. T. Burns, J. Schade, W. A. Brown and K. R. Minor, *Iron & Steelmaker* **19**, 11, 35 (1992).
4. X. Hwang and B. G. Thomas, *Metall. Mater. Trans. B* **27**, 617 (1996).
5. S. Chakrabory and Y. Sahai, *Metall. Trans. B* **23**, 153 (1992).
6. Y. S. Hwang, P. R. Cha, H. S. Nam, K. H. Moon and J. K. Yoon, *ISIJ Int.* **37**, 659 (1997).